

Article

Hybrid Nanofluid Flow and Heat Transfer Past an Inclined Surface

Sumayyah Alabdulhadi ^{1,2}, Iskandar Waini ³, Sameh E. Ahmed ^{4,5}  and Anuar Ishak ^{1,*} 

¹ Department of Mathematical Sciences, Faculty of Science and Technology, Universiti Kebangsaan Malaysia (UKM), Bangi 43600, Selangor, Malaysia; sabdaldhady@qu.edu.sa

² Department of Mathematics, Faculty of Science, Qassim University, Qassim 52571, Saudi Arabia

³ Fakulti Teknologi Kejuruteraan Mekanikal dan Pembuatan, Universiti Teknikal Malaysia Melaka, Hang Tuah Jaya, Durian Tunggal 76100, Melaka, Malaysia; iskandarwaini@utem.edu.my

⁴ Department of Mathematics, Faculty of Science, King Khalid University, Abha 62529, Saudi Arabia; sehassan@kku.edu.sa

⁵ Department of Mathematics, Faculty of Science, South Valley University, Qena 83523, Egypt

* Correspondence: anuar_mi@ukm.edu.my

Abstract: This paper examines the hybrid nanoparticles and the magnetic field impacts on the mixed convection boundary layer flow and heat transfer caused by an inclined shrinking–stretching surface in a hybrid nanofluid. Silver (Ag) is added into a MgO–water nanofluid to form Ag–MgO–water hybrid nanofluid. By making use of proper similarity transformations, the governing equations are transformed to ordinary differential equations. The problem is numerically solved with the help of the MATLAB function bvp4c. The influences of the chosen parameters on the temperature, velocity, heat transfer rate and the skin friction coefficient are addressed and graphically illustrated. The results show that increasing the magnetic parameter substantially improves the heat transfer rate and increases the skin friction coefficient. The findings also suggest that increasing the nanoparticle volume fraction ϕ_2 (Ag) improves the skin friction coefficient while decreasing the heat transfer rate. For both stretching and shrinking instances, non-unique (dual) solutions are discovered. Only the first solution is stable, according to the temporal stability analysis of the dual solutions.

Keywords: stretching–shrinking; hybrid nanofluid; stability analysis; MHD; dual solutions; mixed convection



Citation: Alabdulhadi, S.; Waini, I.; Ahmed, S.E.; Ishak, A. Hybrid Nanofluid Flow and Heat Transfer Past an Inclined Surface. *Mathematics* **2021**, *9*, 3176. <https://doi.org/10.3390/math9243176>

Academic Editor: Andrey Amosov

Received: 4 November 2021

Accepted: 7 December 2021

Published: 9 December 2021

Publisher's Note: MDPI stays neutral with regard to jurisdictional claims in published maps and institutional affiliations.



Copyright: © 2021 by the authors. Licensee MDPI, Basel, Switzerland. This article is an open access article distributed under the terms and conditions of the Creative Commons Attribution (CC BY) license (<https://creativecommons.org/licenses/by/4.0/>).

1. Introduction

Heat transfer enhancement has gained much attention in current years, caused by its numerous uses in engineering and industries. In most applications, heat transfer fluids are utilized as cooling fluids, such as water, paraffin oil, diathermic oil, ethylene glycol, naphthenic mineral oil, vegetable oil, etc. However, these common fluids have poor thermal conductivity, which minimizes the amount of heat transferred. Thus, an innovative method of improving heat transfer in fluids is by adding nanosized particles in the base fluid to create a nanofluid mixture. It was presented by Choi and Eastman [1]. Nanofluids possess a significantly higher thermal conductivity than regular fluids. Therefore, nanofluids are widely used for a wide range of applications, such as nuclear reactor cooling, cooling of vehicles and machinery, electronic device cooling, biomedicine, etc. [2]. Consequently, many researchers have investigated the behaviors and properties of nanofluids for different aspects, numerically and experimentally. For example, Tiwari and Das [3] have proposed mathematical models of nanofluids that study the nanofluids' behavior, considering the solid volume fractions of nanoparticles' effects. The governing equations were numerically solved by the finite volume method (FEM). Several researchers have used the Tiwari–Das nanofluid model extensively; see [4–15].

The study of magnetohydrodynamics (MHD) flow is fundamental in the industry and has applications in a variety of fields, including petroleum products and metallurgical operations [16]. The rate of cooling in these processes has a huge impact on the finished

product's qualities, which can be regulated using a magnetic field and electrically conductive fluids. Various studies looked at the impact of applying a magnetic field on a nanofluid. The stretching surface and convective stagnation point flow of an incompressible nanofluid were used by Tian et al. [17] to study the magnetohydrodynamic flow numerically. The entropy of the boundary layer flow was investigated by Rashid et al. [18] using nanofluid generated by the shrinking porous surface. Moreover, Gopal et al. [19] revealed the effects of electric and magnetic force with viscosity dissipation on nanofluids of higher-order chemical processing over a continuously stretching porous wall. Furthermore, mixed convection flow (forced and free convection flow) has numerous engineering applications, for example, electrical engineering and chemical engineering, to name a few. As a result, numerous experts have looked into the mixed convection flow of nanofluids. The flow of a mixed convection nanofluid boundary layer toward a shrinking–stretching sheet at a stagnation point has been analyzed by Othman et al. [20]. The impact of physical variables on nanofluids' flow, mass transfer, and heat transfer has been studied. Moreover, Ziaei-Rad et al. [21] reviewed the study of the mixed convection boundary layer nanofluid flow past a permeable inclined surface problem. In contrast, the numerical simulation of heat transfer and mixed convection nanofluid flow in a trapezoidal channel in a porous medium was carried out by El-shorbagy et al. [22]. Besides, in nanofluids, several researchers examined the MHD mixed convection flow past a stretching sheet. Over a stretching permeable sheet, Chamkha et al. [23] illustrated the MHD mixed convection nanofluid flow. The impact of viscous dissipation and a changing magnetic field on entropy production in MHD mixed convection nanofluid flow via a non-linear stretching surface were numerically explored by Matin et al. [24]. Besides, Ibrahim et al. [25] examined the impacts of viscous dissipation, thermal radiation, chemical reaction, suction, and heat generation of the MHD mixed convection boundary layer nanofluid flow with a stretching permeable sheet. Additionally, Vasanthakumari and Pondy [26] addressed the MHD mixed convection flow of a nanofluid across the inclined stretching sheet, having internal heat generation taken into account. Moreover, Gupta et al. [27] analyzed the joined impacts of the chemical reaction, magnetic field, and thermal radiation on the mixed convection incompressible nanofluid flow and heat transfer toward a stagnation point across an inclined stretching sheet.

In recent years, scientists and researchers are still looking for a better fluid to replace nanofluid and obtain a highly efficient heat transfer fluid. Their efforts led to the term: hybrid nanofluid. Hybrid nanofluids are an extension of nanofluids that contain two distinct types of nanoparticles mixed together in a base fluid. Hybrid nanofluids can enhance thermal characteristics better than regular nanofluids. The comparison between hybrid and traditional nanofluid in terms of the heat transfer characteristics was made by Devi and Devi [28]. They discovered that the hybrid nanofluid's heat transfer rate is greater than the traditional nanofluid, even in the occurrence of a magnetic field. Furthermore, because of the benefits of hybrid nanofluids, researchers are eager to work toward hybrid nanofluids as heat transfer fluid. For instance, this includes the influence of Cu- Al_2O_3 -water hybrid nanofluid flow and heat transfer along a permeable moving sheet were described by Waini et al. [29]. According to the findings, in comparison to nanofluids containing single type of nanoparticles, hybrid nanofluids improve heat transfer properties. At present, many researchers are interested in the presence of dual solutions for the mixed convection flow. Zainal et al. [30] studied the MHD mixed convection flow across a vertical flat plate in a hybrid nanofluid with convective boundary conditions. They discovered dual solutions in both assisting and opposing flow regions. Waini et al. [31] analyzed the steady flow of mixed convection hybrid nanofluids over a vertical surface in a porous medium. Several dual solutions were found within a specific set of buoyancy parameters. Furthermore, the usage of hybrid nanoparticles causes the boundary layer to separate more slowly. Rostami et al. [32] evaluated the steady laminar MHD-mixed convection stagnation point flow over a vertical permeable flat plate in a hybrid nanofluid. Within a specific range of the buoyancy parameter, dual solutions have been reported, and the stability of these solutions has been determined. Jamaludin et al. [33] examined the MHD mixed

convection stagnation point flow and heat transfer in Cu-Al₂O₃-water hybrid nanofluid above a permeable shrinking–stretching surface. Thus, a full report on the behavior of both lower and higher branch solutions was presented. The dual solutions were determined by Khashi'ie et al. [34] when they used hybrid nanofluids to study the mixed convection flow via a vertical plate embedded in a porous medium.

A numerical study of a hybrid nanofluid flow problem over a stretching–shrinking sheet has grabbed scientists' and researchers' intension in recent years. In a hybrid nanofluid, Waini et al. [35] carried out a numerical analysis of the unsteady flow and heat transfer toward a shrinking–stretching surface. They concluded that the velocity for Cu-Al₂O₃-water hybrid nanofluid increases with the increase in the suction parameter. They also discovered that the use of the hybrid nanofluid under the influence of the suction force could cause a further decrease in the temperature. Khashi'ie et al. [36] numerically investigated the impact of the convective condition and velocity slip on the three-dimensional hybrid nanofluids flow past a stretching–shrinking surface. They discovered that the increase in Biot and slip parameters can improve the heat transfer rates, but increasing the copper solid volume fraction has the opposite effect. In addition, using an Ag-MgO-water hybrid nanofluid, a numerical examination of the influence of boundary layer flow and heat transfer past an inclined permeable stretching–shrinking surface was carried out by Anuar et al. [37]. They found that when the angle of inclination and suction parameters increase, the local Nusselt number rises. The findings also show that raising the volume fraction of Ag nanoparticles in MgO-water nanofluid reduces the local Nusselt number. Furthermore, the hybrid nanofluid flow problem past a stretching–shrinking sheet was revealed numerically by Roşca and Pop [38], Anuar et al. [39], Wahid et al. [40] and Waini et al. [41], taking into account the various physical parameters.

Motivated by the above literature, the flat plate has been used in several research articles in two different positions; horizontal and vertical. Conversely, the inclined flat plate has received less interest. Nevertheless, there has never been a study of MHD mixed convection on an inclined stretching–shrinking sheet employing a hybrid nanofluid. As a result of the knowledge gap mentioned above, the current study attempts to enhance the work of Anuar et al. [37]. It can be performed by examining the MHD mixed convection flow of a hybrid nanofluid over an inclined permeable stretching–shrinking surface with suction force effects. The present model considers the solid volume fractions of nanoparticles while examining hybrid nanofluid behavior. The base fluid contains two distinct nanoparticles (Ag and MgO). Utilizing the similarity transformation approach, the governing equations with boundary conditions are transformed into a system of ordinary differential equations. The equations system is then solved using the MATLAB boundary value problem solver (bvp4c). In tabular and graphical representations, the impacts of many physical factors on heat transfer and flow characteristics are presented and explained. The stability analysis is carried out once the dual solutions for both stretching and shrinking instances are found. Furthermore, the difference has been presented with the previously published data to validate the obtained numerical results.

2. Formulation of the Problem

The mixed convection of magnetohydrodynamic flow of a hybrid nanofluid induced by an inclined permeable stretching–shrinking surface with an angle of inclination α as displayed in Figure 1 is considered, where x - and y -axes are the dimensional Cartesian coordinates. Here, the x -axis extends along the plate while the y -axis normal to it. We assume that the velocity of the stretching–shrinking surface is $u_w(x) = ax$, where a is a positive constant. Additionally, the surface temperature of the sheet is considered as $T_w(x) = T_\infty + bx$, where b is a constant and the constant ambient temperature is signified as T_∞ . In addition, $v_w(x)$ denotes the mass flux velocity. A uniform magnetic field B_0 is applied normal to the plate. Meanwhile, the size of nanoparticles in the hybrid nanofluid is assumed to be uniform, and the agglomeration effect is neglected since the hybrid nanofluid is formed as a stable compound. Under the presumptions outlined above, the governing

boundary layer equations of the hybrid nanofluid by employing the usual approximations of the boundary layer for the continuity, momentum and energy equations can be written as (see Devi and Devi [28], Afridi et al. [42] and Anuar et al. [37]):

$$\frac{\partial u}{\partial x} + \frac{\partial v}{\partial y} = 0 \tag{1}$$

$$u \frac{\partial u}{\partial x} + v \frac{\partial u}{\partial y} = \frac{\mu_{hnf}}{\rho_{hnf}} \frac{\partial^2 u}{\partial y^2} + \frac{(\rho\beta)_{hnf}}{\rho_{hnf}} g(T - T_\infty) \cos \alpha - \frac{\sigma_{hnf} B_0^2 u}{\rho_{hnf}} \tag{2}$$

$$u \frac{\partial T}{\partial x} + v \frac{\partial T}{\partial y} = \frac{k_{hnf}}{(\rho c_p)_{hnf}} \frac{\partial^2 T}{\partial y^2}, \tag{3}$$

subject to the boundary conditions [37]:

$$\begin{aligned} v = v_w, \quad u = u_w \varepsilon, \quad T = T_w(x) \text{ at } y = 0 \\ u \rightarrow 0, \quad T \rightarrow T_\infty \text{ as } y \rightarrow \infty, \end{aligned} \tag{4}$$

where u and v are the hybrid nanofluid velocity components along x and y directions. Here, T signifies the temperature of the hybrid nanofluid, α denotes the inclination angle, B_0 symbolizes the uniform magnetic field, g implies the acceleration due to gravity and ε represents the parameter of the stretching–shrinking sheet with $\varepsilon < 0$ and $\varepsilon > 0$ are for the shrinking and stretching sheets, respectively, while $\varepsilon = 0$ for the static surface. Meanwhile, μ_{hnf} , ρ_{hnf} , k_{hnf} , σ_{hnf} , $(\rho\beta)_{hnf}$, and $(\rho c_p)_{hnf}$ are the dynamic viscosity, density, thermal conductivity, electrical conductivity, thermal expansion coefficient and heat capacity of the Ag-MgO–water hybrid nanofluid, respectively, which have the following definitions (see Devi and Devi [28]):

$$\begin{aligned} \mu_{hnf} &= \frac{\mu_f}{(1-\varphi_1)^{2.5}(1-\varphi_2)^{2.5}}, \quad \rho_{hnf} = (1 - \varphi_2) \left[(1 - \varphi_1)\rho_f + \varphi_1\rho_1 \right] + \varphi_2\rho_2, \\ (\rho c_p)_{hnf} &= \varphi_2(\rho c_p)_2 + (1 - \varphi_2) \left[(1 - \varphi_1)(\rho c_p)_f + \varphi_1(\rho c_p)_1 \right], \\ (\rho\beta)_{hnf} &= \varphi_2(\rho\beta)_2 + (1 - \varphi_2) \left[(1 - \varphi_1)(\rho\beta)_f + \varphi_1(\rho\beta)_1 \right], \\ \frac{k_{hnf}}{k_{bf}} &= \frac{k_2 + 2k_{bf} - 2\varphi_2(k_{bf} - k_2)}{k_2 + 2k_{bf} + \varphi_2(k_{bf} - k_2)} \text{ where } \frac{k_{bf}}{k_f} = \frac{k_1 + 2k_{bf} - 2\varphi_1(k_f - k_1)}{k_1 + 2k_f + \varphi_1(k_f - k_1)} \\ \frac{\sigma_{hnf}}{\sigma_f} &= \frac{\sigma_2 + 2\sigma_{bf} - 2\varphi_2(\sigma_{bf} - \sigma_2)}{\sigma_2 + 2\sigma_{bf} + \varphi_2(\sigma_{bf} - \sigma_2)} \text{ where } \frac{\sigma_{bf}}{\sigma_f} = \frac{\sigma_1 + 2\sigma_f - 2\varphi_1(\sigma_f - \sigma_1)}{\sigma_1 + 2\sigma_f + \varphi_1(\sigma_f - \sigma_1)} \end{aligned} \tag{5}$$

where the subscripts 1 and 2 represent MgO solid fraction and Ag solid fraction, while the subscripts hnf and f symbolize hybrid nanofluid and fluid, respectively. Furthermore, φ_1 and φ_2 indicate the volume fractions of MgO and Ag nanoparticles, respectively, where $\varphi_1 = \varphi_2 = 0$ signifies the regular fluid. The required hybrid nanofluid is formed by adding Ag nanoparticles into MgO–water. The thermophysical properties of silver (Ag), magnesium oxide (MgO) and water (H₂O) are provided in Table 1, as reported by Abu-Libdeh et al. [43], Khan et al. [44] and Ghalambaz et al. [45]. As stated in [45], the thermal conductivity of the hybrid nanofluid is evaluated through curve fitting of the experimental data of Esfe et al. [46].

Table 1. The physical thermal characteristics of nanoparticles and water.

Physical Properties	MgO	Water	Ag
ρ (kg m ⁻³)	3580	997.1	10,500
c_p (J kg ⁻¹ K ⁻¹)	879	4179	235
k (W m ⁻¹ K ⁻¹)	30	0.613	429
β (K ⁻¹)	33.6×10^{-6}	21×10^{-5}	5.4×10^{-5}
σ (s/m)	8×10^{-4}	5.5×10^{-6}	8.1×10^{-4}

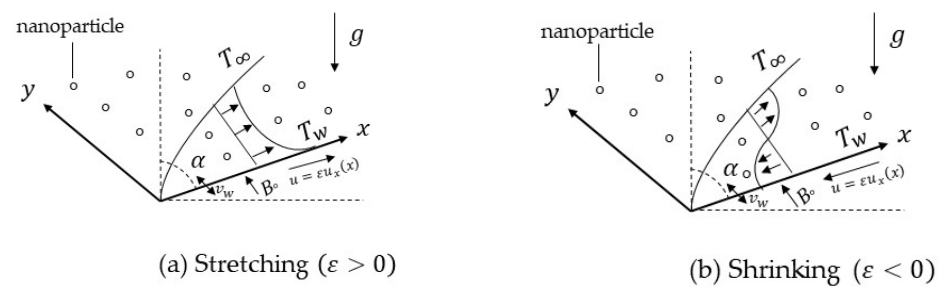


Figure 1. The schematic problem flow. Following Anuar et al. [37], to obtain the similarity solutions for the Equations (1)–(4), the appropriate similarity transformations are employed as follows:

$$\psi = \sqrt{av_f}xf(\eta), \quad \eta = \sqrt{\frac{a}{v_f}}y, \quad \theta(\eta) = \frac{T - T_\infty}{T_w(x) - T_\infty} \tag{6}$$

where f signifies as dimensionless velocity, θ symbolizes the dimensionless temperature, η and v_f are the similarity variable and the kinematic viscosity, respectively. Meanwhile, ψ is the stream function and the components of velocity are defined as $u = \frac{\partial\psi}{\partial y}$ and $v = -\frac{\partial\psi}{\partial x}$. Utilizing these definitions, the continuity Equation (1) is fully satisfied, and the velocities are expressed as:

$$u = axf'(\eta), \quad v = -\sqrt{av_f}f(\eta), \tag{7}$$

such that:

$$v_w = -\sqrt{av_f}s \tag{8}$$

Here, s indicates the constant mass flux parameter where $s < 0$ for injection and $s > 0$ for suction.

Substituting the similarity variables (6) into governing Equations (2) and (3), one obtains the following similarity equations:

$$\frac{\mu_{hnf}/\mu_f}{\rho_{hnf}/\rho_f}f''' - f'^2 + ff'' + \frac{(\rho\beta)_{hnf}/(\rho\beta)_f}{\rho_{hnf}/\rho_f}\lambda\theta\cos\alpha - \frac{\sigma_{hnf}/\sigma_f}{\rho_{hnf}/\rho_f}Mf' = 0, \tag{9}$$

$$\frac{1}{Pr} \frac{k_{hnf}/k_f}{(\rho c_p)_{hnf}/(\rho c_p)_f} \theta'' + f\theta' - f'\theta = 0. \tag{10}$$

The boundary conditions (4) are converted to:

$$\begin{aligned} f'(0) &= \varepsilon, \quad f(0) = s, \quad \theta(0) = 1. \\ f'(\eta) &\rightarrow 0, \quad \theta(\eta) \rightarrow 0 \text{ as } \eta \rightarrow \infty \end{aligned} \tag{11}$$

Note that $\lambda = Gr/Re_x^2$ is the mixed convection parameter or the buoyancy parameter, where $Gr = g\beta_f(T_w(x) - T_\infty)x^3/v_f^2$ is the Grashof number and $Re_x = u_w(x)x/v_f$ represents the local Reynold number. Furthermore, $\lambda < 0$ demonstrates the opposing buoyancy force while $\lambda > 0$ signifies the assisting buoyancy force. Moreover, $M = \sigma_f B_0^2/\alpha_f$ and $Pr = v_f/\alpha_f$ are the magnetic parameter and the Prandtl number, respectively.

Next, the local Nusselt number (Nu_x) and the skin friction coefficient (c_f) are the parameters of physical interest, which can be defined as follows:

$$Nu_x = -\frac{xk_{hnf}}{k_f(T_w - T_\infty)} \left(\frac{\partial T}{\partial y} \right)_{y=0}, \quad C_f = \frac{\mu_{hnf}}{\rho_f u_w^2} \left(\frac{\partial u}{\partial y} \right)_{y=0}. \tag{12}$$

By substituting (6) into Equation (12), one obtains:

$$Re_x^{1/2} C_f = \frac{\mu_{hmf}}{\mu_f} f''(0), \quad Re_x^{-1/2} Nu_x = -\frac{k_{hmf}}{k_f} \theta'(0) \tag{13}$$

3. Stability Analysis

The numerical results reveal that there are non-uniqueness solutions from the boundary value problem (9)–(11) for a specific value of the physical parameters. As a result, a stability analysis, as shown in Merkin [47] as well as Weidman et al. [48], is used to identify the most trustworthy and stable solution and thus physically reliable. We have,

$$\frac{\partial u}{\partial t} + u \frac{\partial u}{\partial x} + v \frac{\partial u}{\partial y} = \frac{\mu_{hmf}}{\rho_{hmf}} \frac{\partial^2 u}{\partial y^2} + \frac{(\rho\beta)_{hmf}}{\rho_{hmf}} g(T - T_\infty) \cos \alpha - \frac{\sigma_{hmf} B_0^2 u}{\rho_{hmf}} \tag{14}$$

$$\frac{\partial T}{\partial t} + u \frac{\partial T}{\partial x} + v \frac{\partial T}{\partial y} = \frac{k_{hmf}}{(\rho c_p)_{hmf}} \frac{\partial^2 T}{\partial y^2} \tag{15}$$

thus, the new dimensionless time variable τ is considered. By using variables in (6), the new similarity variables are introduced as:

$$\psi = \sqrt{av_f} x f(\eta, \tau), \quad \eta = \sqrt{\frac{a}{v_f}} y, \quad \theta(\eta, \tau) = \frac{T - T_\infty}{T_w(x) - T_\infty}, \quad \tau = at \tag{16}$$

Applying Equation (16) into Equations (14) and (15), the following system of equations are attained:

$$\frac{\mu_{hmf}/\mu_f}{\rho_{hmf}/\rho_f} \frac{\partial^3 f}{\partial \eta^3} - \left(\frac{\partial f}{\partial \eta}\right)^2 + f \frac{\partial^2 f}{\partial \eta^2} + \frac{(\rho\beta)_{hmf}/(\rho\beta)_f}{\rho_{hmf}/\rho_f} \lambda \theta \cos \alpha - \frac{\sigma_{hmf}/\sigma_f}{\rho_{hmf}/\rho_f} M \frac{\partial f}{\partial \eta} - \frac{\partial^2 f}{\partial \eta \partial \tau} = 0 \tag{17}$$

$$\frac{1}{Pr} \frac{k_{hmf}/k_f}{(\rho c_p)_{hmf}/(\rho c_p)_f} \frac{\partial^2 \theta}{\partial \eta^2} + f \frac{\partial \theta}{\partial \eta} - \frac{\partial f}{\partial \eta} \theta - \frac{\partial \theta}{\partial \tau} = 0 \tag{18}$$

With the following initial and boundary conditions:

$$\begin{aligned} \frac{\partial f}{\partial \eta}(0, \tau) &= \varepsilon, \quad f(0, \tau) = s, \quad \theta(0, \tau) = 1, \\ \frac{\partial f}{\partial \eta}(\eta, \tau) &\rightarrow 0, \quad \theta(\eta, \tau) \rightarrow 0, \quad \text{as } \eta \rightarrow \infty \end{aligned} \tag{19}$$

Following Weidman et al. [48], to examine the stability of the dual solutions $f(\eta) = f_0(\eta)$ and $\theta(\eta) = \theta_0(\eta)$, we write:

$$\theta(\eta, \tau) = \theta_0(\eta) + e^{-\gamma\tau} G(\eta, \tau), \quad f(\eta, \tau) = f_0(\eta) + e^{-\gamma\tau} F(\eta, \tau), \tag{20}$$

by which γ is an unknown eigenvalue parameter, while functions $F(\eta)$ and $G(\eta)$ are small relative to $f_0(\eta)$ and $\theta_0(\eta)$, respectively. Thus, by substituting Equation (20) into (17) and (18) along with the conditions (19), and by taking $\tau = 0$, we can express the linear eigenvalue problem as follows:

$$\frac{\mu_{hmf}/\mu_f}{\rho_{hmf}/\rho_f} F_0''' + f_0 F_0'' + F_0 f_0'' + \frac{(\rho\beta)_{hmf}/(\rho\beta)_f}{\rho_{hmf}/\rho_f} \lambda G_0 \cos \alpha - \left(2f_0' - \gamma + \frac{\sigma_{hmf}/\sigma_f}{\rho_{hmf}/\rho_f} M\right) F_0' = 0 \tag{21}$$

$$\frac{1}{Pr} \frac{k_{hmf}/k_f}{(\rho c_p)_{hmf}/(\rho c_p)_f} G_0'' + f_0 G_0' + F_0 \theta_0' - f_0' G_0 - F_0' \theta_0 + \gamma G_0 = 0 \tag{22}$$

Subject to the linearized conditions:

$$\begin{aligned} F_0'(0) &= 0, \quad F_0(0) = 0, \quad G_0(0) = 0, \\ F_0'(\eta) &\rightarrow 0, \quad G_0(\eta) \rightarrow 0 \quad \text{as } \eta \rightarrow \infty \end{aligned} \tag{23}$$

Following Harris et al. [49], resting the boundary condition on $F_0(\eta)$ leads to the determination of the smallest eigenvalues γ . In the current work, the condition $F_0'(\eta) \rightarrow 0$ as $\eta \rightarrow \infty$ is relaxed, which is replaced by the new boundary condition $F_0''(0) = 1$.

4. Numerical Method

The governing Equations (9) and (10) subject to the boundary restrictions (11) are solved numerically by the aid of the `bvp4c` function in MATLAB software. The `bvp4c` solver is explained in detail by Shampine et al. [50]. This solver uses the finite difference method that implements the three stages of the Lobatto IIIa formula. The syntax of the solver is defined by “`sol=bvp4c (@OdeBVP, @OdeBC, solinit, options)`”. To start the `bvp4c` routine, we need to convert Equations (9) and (10) into a system of first-order ordinary differential equations and rewrite them as follows:

$$f = y(1), f' = y(2), f'' = y(3), \theta = y(4), \theta' = y(5)$$

$$f''' = \frac{\rho_{hnf}/\rho_f}{\mu_{hnf}/\mu_f} \left(y(2)y(2) - y(1)y(3) - \frac{(\rho\beta)_{hnf}/(\rho\beta)_f}{\rho_{hnf}/\rho_f} \lambda y(4) \cos \alpha + \frac{\sigma_{hnf}/\sigma_f}{\rho_{hnf}/\rho_f} My(2) \right) \quad (24)$$

$$\theta'' = Pr \frac{(\rho c_p)_{hnf}/(\rho c_p)_f}{k_{hnf}/k_f} (y(2)y(4) - y(1)y(5)). \quad (25)$$

The initial and boundary conditions (11) become:

$$ya(1) - s, ya(2) - \varepsilon, ya(4) - 1, yb(2), \theta b(4) \quad (26)$$

The dual solutions are explored using two different initial guesses for the values of $-\theta'(0)$ and $f''(0)$. The appropriate initial guess and thickness of the boundary layer, η_∞ must be chosen relying on the parameters applied, to obtain the required results. To validate the current numerical procedure, the values of $f''(0)$ are compared to cases that have been reported in Roşca and Pop [51] and Anuar et al. [37] for regular fluid ($\varphi_1 = \varphi_2 = 0$) with various values of ε and s when $\lambda = 0, M = 0$ and $\alpha = 90^\circ$ as elucidated in Table 2, which shows a favorable agreement. Additionally, Table 3 compares the values of $-\theta'(0)$ for regular fluid ($\varphi_1 = \varphi_2 = 0$) for various values of λ when $\varepsilon = 1, s = 0, M = 0, \alpha = 0^\circ$ and $Pr = 1$ with those reported in Roşca and Pop [51] and Anuar et al. [37]. As a result, these tables indicate that the current results are valid and reliable. Thus, we can conclude that the developed algorithm for studying numerically the hybrid nanofluids flow can be used with great confidence.

Table 2. Comparison of $f''(0)$ when ($\varphi_1 = \varphi_2 = 0$) with diverse values of ε and s when $\lambda = 0, M = 0$ and $\alpha = 90^\circ$.

ε	s	Present Result	Anuar et al. [37]	Roşca and Pop [51]
1	2.0	−2.414214	−2.414214	−2.4142
	2.5	−2.850781	−2.850781	−2.8507
	3.0	−3.302776	−3.302776	−3.3027
	3.5	−3.765564		
−1	2.0	1.010530	1.010532	1.0106
	2.5	2.000000	2.000000	2.0000
	3.0	2.618034	2.618034	2.6180
	3.5	3.186141		

Table 3. Comparison of $-\theta'(0)$ when $(\varphi_1 = \varphi_2 = 0)$ with diverse values of λ when $\varepsilon = 1, s = 0, M = 0, \alpha = 0^\circ$ and $Pr = 1$.

λ	Present Result	Anuar et al. [37]	Roşca and Pop [51]
0	1.000008	1.000008	1.0000
1	1.087275	1.087275	1.0872
5	1.252700		
10	1.371564	1.371564	1.3715

5. Results

The present work aims to investigate the influence of governing parameters such as suction parameter, s , nanoparticle volume fraction parameter, φ_1, φ_2 , mixed convection parameter, λ , stretching–shrinking parameter, ε , magnetic parameter, M , and inclination angle parameter, α , on the reduced skin friction $f''(0)$ and the reduced Nusselt number $-\theta'(0)$ which are presented in Figures 2 and 3 as well as the dimensionless velocity $f'(\eta)$ and temperature $\theta(\eta)$ which are displayed in Figures 4 and 5. From these figures, it can be seen that two solutions exist for Equations (9)–(11) in the range of $\varepsilon < \varepsilon_C$ for both inclined permeable stretching and shrinking sheet, a unique solution found when $\varepsilon = \varepsilon_C$ and no solution is obtained when $\varepsilon > \varepsilon_C$, where ε_c signifies the critical value of ε which the dual solutions are joined.

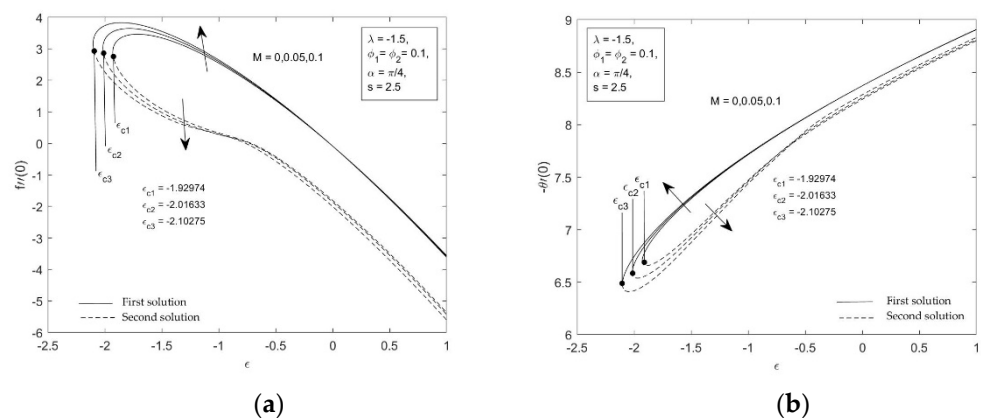


Figure 2. Skin friction coefficient $f''(0)$ and local Nusselt number $-\theta'(0)$ against ε for various values of M .

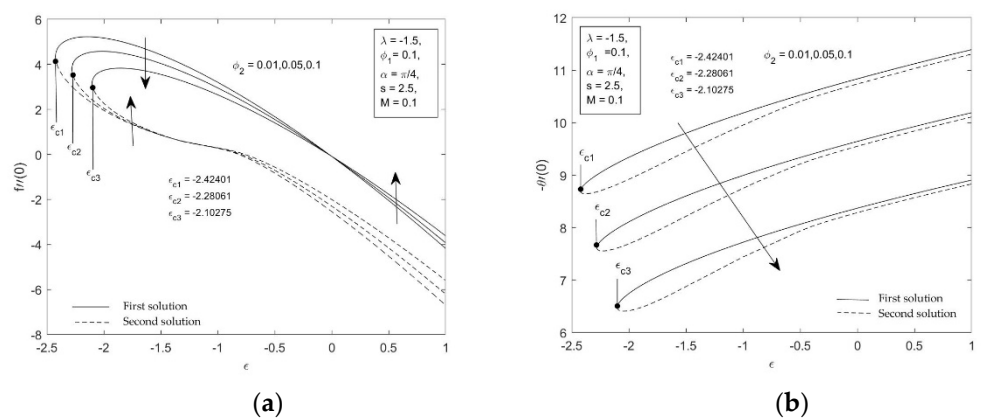


Figure 3. Skin friction coefficient $f''(0)$ local Nusselt number $-\theta'(0)$ against ε for various values of φ_2 .

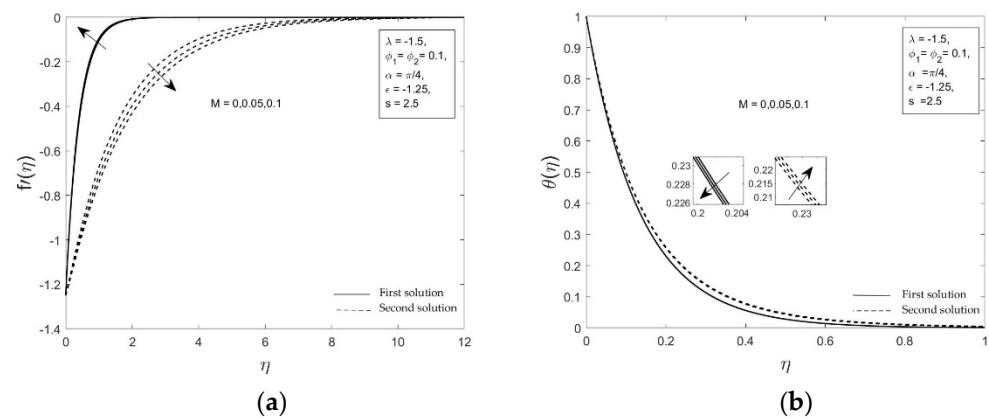


Figure 4. Velocity profiles $f'(\eta)$ and temperature profiles $\theta(\eta)$ for various values of M .

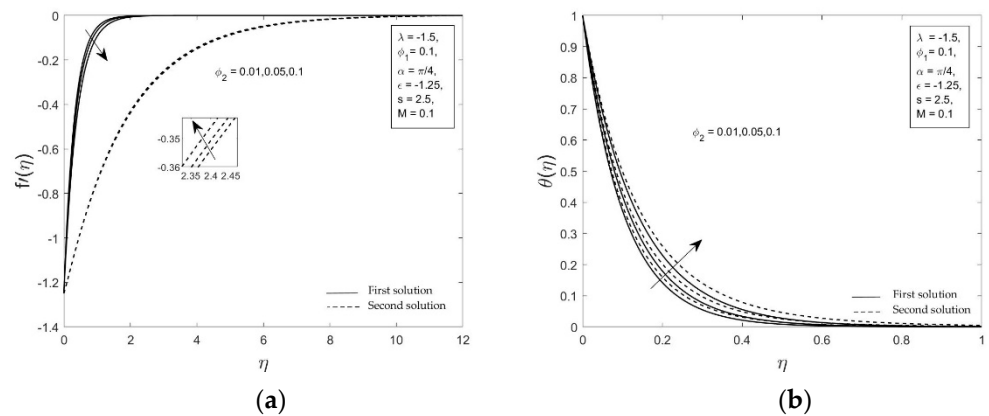


Figure 5. Velocity profiles $f'(\eta)$ and temperature profiles $\theta(\eta)$ for various values of φ_2 .

For more details, Figure 2 displays the effect of M on the reduced skin friction $f''(0)$ and the reduced Nusselt number $-\theta'(0)$ against ε when $Pr = 6.2$, $\varphi_1 = \varphi_2 = 0.1$, $\alpha = \pi/4$, $\lambda = -1.5$ and $s = 2.5$. It can be seen that the rise of M augments both $f''(0)$ and $-\theta'(0)$ because of the reverse force known as the Lorentz force. As a result of the resistance to the motion of the fluid particles, this force appears to reduce fluid velocity. The synchronization of the magnetic and electric fields resulting from the creation of the Lorentz force appears to slow down the fluid movement. The boundary layer is becoming increasingly thin (see Figure 4a) as M upsurges due to the postponed flow, thus increasing of $f''(0)$ and $-\theta'(0)$. From these figures, the behavior of the critical value of the stretching–shrinking parameter ε is going down with the incrementing of M . The critical values of ε for $M = 0, 0.05, 0.1$ are $\varepsilon_c = -1.92974, -2.01633$ and -2.10275 , respectively.

The variations of the reduced skin friction coefficient $f''(0)$ and the reduced Nusselt number $-\theta'(0)$ with some rates of ε together with three varying values of solid volume fraction $\varphi_2 = 0.01, 0.05, 0, 1$, are illustrated in Figure 3 where $Pr = 6.2$, $\varphi_1 = 0.1$, $\alpha = \pi/4$, $M = 0.1$, $\lambda = -1.5$ and $s = 2.5$. Figure 3a highlights that the value of $f''(0)$ is increasing for the second solution; however, dual behaviors are found for the first solution of $f''(0)$, where these values are decrementing at the shrinking region ($\varepsilon < 0$) but increasing at the stretching region ($\varepsilon > 0$) when the value of φ_2 boosts, because of the increase in the volume fraction of nanoparticles raises the viscosity of the fluid. Hence, this helped to recover the coefficient of the skin friction along the surface. Moreover, Figure 3b conveys that the reduced Nusselt number (heat transfer rate) is reduced as the nanoparticle volume fraction augments for both inclined stretching and shrinking surfaces. Meanwhile, the values of $f''(0)$ appear to increase with the decrease of ε , but for $-\theta'(0)$, the opposite trend is observed. The critical values of ε are observed for solid volume fraction $\varphi_2 = 0.01, 0.05, 0, 1$ where $\varepsilon_c = -2.42401, -2.28061$ and -2.10275 , respectively.

The profiles of $f'(\eta)$ and $\theta(\eta)$ for certain physical parameters are presented in Figures 4 and 5. From these figures, it is noticeable that there are dual solutions for the velocity profiles $f'(\eta)$ and the temperature profiles $\theta(\eta)$, which asymptotically satisfy the conditions (11), indicating that the current numerical findings are valid. The distribution of velocity profiles $f'(\eta)$ and the temperature profiles $\theta(\eta)$ for numerous values of the magnetic parameter M when $\lambda = -1.5$, $\varphi_1 = \varphi_2 = 0.1$, $\alpha = \pi/4$, $\varepsilon = -1.25$ and $s = 2.5$ are presented in Figure 4. As seen in Figure 4a, the velocity $f'(\eta)$ appears to increase with the increase of M for the first solution. Furthermore, a different direction is observed for the second solution. Meanwhile, Figure 4b exposes that the rise in M causes a decrease in the temperature for the first solution, whereas an increment activity is preserved in the second solution. The Lorentz force is a resistive force that resists the fluid movement, resulting in decreasing manner of the velocity and the temperature for the first solutions, as shown in Figure 4. As a result, the velocity gradient as well as the temperature gradient at the surface increases, which in turn increases the skin friction coefficient and the Nusselt number. These findings are in agreement with the outcomes presented in Figure 2. Conversely, the second solutions show a different behavior, which is related to the stability of the solution that will be explained later.

Figure 5 shows the solid volume fraction φ_2 effect toward the velocity profiles $f'(\eta)$ and the temperature profiles $\theta(\eta)$ when $\lambda = -1.5$, $\varphi_1 = 0.1$, $\alpha = \pi/4$, $\varepsilon = -1.25$, $M = 0.1$ and $s = 2.5$. As depicted in Figure 5a, the velocity increases in absolute sense for the first solution. This outcome demonstrates that the momentum boundary layer thickness increases in response to the increase of φ_2 , thus reducing the magnitude of the velocity gradient at the surface. This finding is due to the opposing flow caused by the buoyancy force (represented by $\lambda = -1.5$). However, Figure 5b shows that the rise in φ_2 significantly raises the temperature $\theta(\eta)$ for both solutions. The magnification of the nanoparticle volume fraction φ_2 enhances the thermal conductivity of hybrid nanofluid, thus raising the temperature, which in turn reduces the magnitude of the temperature gradient at the surface, $|\theta'(0)|$. Thus, the Nusselt number, which represents the heat transfer rate at the surface decreases as φ_2 increases. This finding is consistent with the results presented in Figure 3b.

The present mathematical model can be applied to predict the results of experiment works. Moreover, the present study also investigates the stability of the solutions in the long run. Figure 6 shows the variations of the eigenvalues γ against λ , while the other parameters are fixed. Referring to Equation (20), the unsteady (time dependent) solution converges to the steady (time independent) state solution as time evolves ($\tau \rightarrow \infty$) if γ is positive. In contrast, the solution diverges if $\gamma < 0$. The sign of γ determines either decay or growth of the disturbance, which then determines the flow stability as time passes. It is evident from Figure 6 that γ is positive for the first solution, while it is negative for the second solution. Therefore, the first solution is stable and thus physically reliable as $\tau \rightarrow \infty$, while the second solution is not. Spangenberg et al. [52] have reported in their experimental work on turbulent boundary layer under strong adverse pressure gradient that dual solutions were obtained as a function of how the pressure gradient was realized. Another example of non-unique flow was reported by Aidun et al. [53], where they observed experimentally that the primary steady state flow in a through-flow lid-driven cavity was non-unique and only one of the multiple steady-state patterns can stabilize in the cavity. Although the second solutions are deprived of physical significance, they are still of interest from mathematical point of view. These solutions are also solutions to the differential equations, which satisfy the far field boundary conditions asymptotically. Similar equations may arise in other situations, where the lower branch solutions could have more realistic meaning [54].

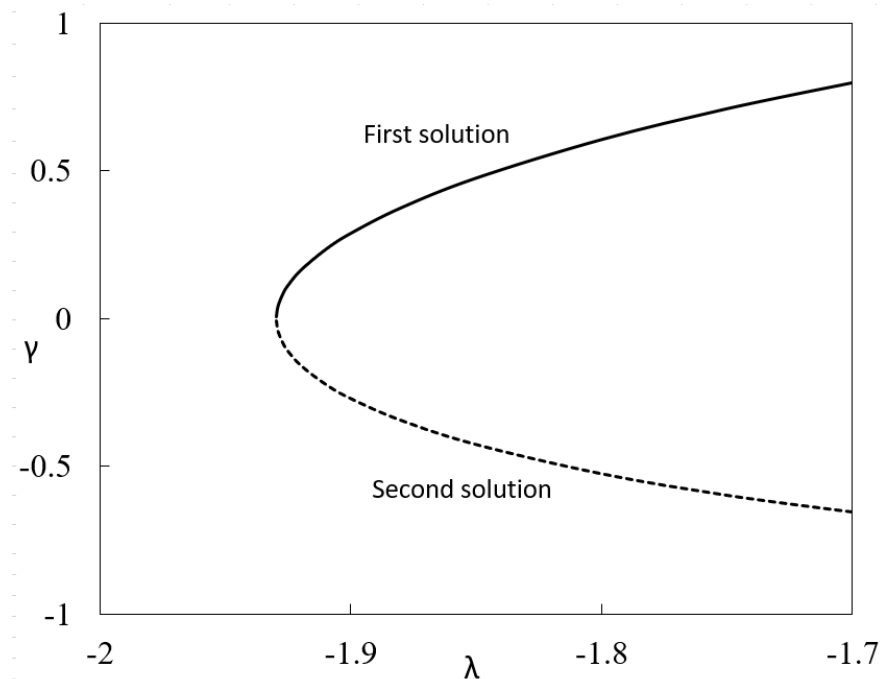


Figure 6. Plot of eigenvalue γ against λ for $Pr = 6.2$, $S = 2.5$, $M = 0.1$, $\varepsilon = -1.5$, $\alpha = \pi/4$, $\varphi_1 = 0.1$ and $\varphi_2 = 0.1$.

6. Conclusions

The MHD mixed convection flow problem past an inclined permeable shrinking–stretching surface in a hybrid Ag-MgO–water nanofluid was investigated. Similarity transformations were utilized to help in obtaining the similarity equations. These equations were solved numerically using the MATLAB program’s boundary value problem solver, *bvp4c*. The significant findings are summarized as follows:

- Dual solutions are found for both stretching and shrinking scenarios ($\varepsilon_c < \varepsilon < 1$), while the solutions came together at $\varepsilon = \varepsilon_c$. Furthermore, there are no solutions for $\varepsilon < \varepsilon_c$.
- The temporal stability analysis shows that only the first solution is stable over time.
- Deferred boundary layer separation occurs in the presence of nanoparticle volume fraction as well as the magnetic parameter.
- The temperature and velocity increase by raising the nanoparticle volume fraction φ_2 and magnetic parameter M .
- The skin friction coefficient as well as the heat transfer rate increases dramatically as magnetic parameter M is raised.
- The augmentation of the nanoparticle volume fraction φ_2 increases the skin friction coefficient but slows down the heat transmission across the inclined shrinking surface.

Author Contributions: Conceptualization, A.I.; funding acquisition, A.I.; methodology, S.A. and I.W.; Supervision, A.I. and S.E.A.; validation, I.W.; writing—original draft, S.A.; writing—review and editing, A.I., I.W. and S.E.A. All authors have read and agreed to the published version of the manuscript.

Funding: This research was funded by Universiti Kebangsaan Malaysia (project code: DIP-2020-001).

Institutional Review Board Statement: Not applicable.

Informed Consent Statement: Not applicable.

Acknowledgments: The financial supports received from the Universiti Kebangsaan Malaysia (Project Code: DIP-2020-001) and the Universiti Teknikal Malaysia Melaka are gratefully acknowledged.

Conflicts of Interest: The authors declare no conflict of interest.

Nomenclature

a, b	positive constants
B_0	uniform magnetic field
C_f	skin friction coefficient
c_p	specific heat at constant pressure ($\text{J kg}^{-1} \text{K}^{-1}$)
f	dimensionless velocity
g	acceleration due to gravity
Gr	Grashof number
k	thermal conductivity of the fluid ($\text{Wm}^{-1} \text{K}^{-1}$)
M	magnetic parameter
Nu_x	local Nusselt number
Pr	Prandtl number
Re_x	local Reynold number
S	constant mass flux parameter
t	time (s)
T	fluid temperature (K)
T_w	surface temperature (K)
T_∞	ambient temperature (K)
u, v	elements of velocity in x and y directions, respectively (ms^{-1})
u_w	velocity of the stretching–shrinking surface (ms^{-1})
v_w	mass flux velocity (ms^{-1})
x, y	Cartesian coordinates (m)

Greek symbols

β	thermal expansion coefficient (K^{-1})
γ	eigenvalue
ε	parameter of stretching–shrinking sheet
η	similarity variable
θ	dimensionless temperature
λ	mixed convection parameter
μ	dynamic viscosity of the fluid ($\text{kg m}^{-1} \text{s}^{-1}$)
ν	kinematic viscosity of the fluid ($\text{m}^2 \text{s}^{-1}$)
ρ	Density of the fluid (kg m^{-3})
(ρc_p)	heat capacity of the fluid ($\text{J K}^{-1} \text{m}^{-3}$)
σ	electrical conductivity of the fluid (S m^{-1})
τ	dimensionless time variable
φ_1	nanoparticle volume fractions for MgO (magnesium oxide)
φ_2	nanoparticle volume fractions for Ag (silver)
ψ	stream function

Subscripts

f	base fluid
nf	nanofluid
hnf	hybrid nanofluid
1	first nanoparticle (MgO)
2	second nanoparticle (Ag)

References

- Choi, S.U.S.; Eastman, J.A. Enhancing Thermal Conductivity of Fluids with Nanoparticles. In Proceedings of the 1995 International Mechanical Engineering Congress and Exhibition, San Francisco, CA, USA, 12–17 November 1995; Volume 66, pp. 99–105.
- Wong, K.V.; De Leon, O. Applications of nanofluids: Current and future. *Nanotechnol. Energy* **2017**, 105–132. [[CrossRef](#)]
- Tiwari, R.K.; Das, M.K. Heat transfer augmentation in a two-sided lid-driven differentially heated square cavity utilizing nanofluids. *Int. J. Heat Mass Transf.* **2007**, 50, 2002–2018. [[CrossRef](#)]
- Sheremet, M.A.; Pop, I.; Nazar, R. Natural convection in a square cavity filled with a porous medium saturated with a nanofluid using the thermal nonequilibrium model with a Tiwari and Das nanofluid model. *Int. J. Mech. Sci.* **2015**, 100, 312–321. [[CrossRef](#)]
- Mehmood, A.; Iqbal, M.S. Heat transfer analysis in natural convection flow of nanofluid past a wavy cone. *J. Mol. Liq.* **2016**, 223, 1178–1184. [[CrossRef](#)]

6. Dinarvand, S.; Hosseini, R.; Pop, I. Axisymmetric mixed convective stagnation-point flow of a nanofluid over a vertical permeable cylinder by Tiwari-Das nanofluid model. *Powder Technol.* **2017**, *311*, 147–156. [[CrossRef](#)]
7. Dinarvand, S.; Pop, I. Free-convective flow of copper/water nanofluid about a rotating down-pointing cone using Tiwari-Das nanofluid scheme. *Adv. Powder Technol.* **2017**, *28*, 900–909. [[CrossRef](#)]
8. Hayat, T.; Ijaz, M.; Qayyum, S.; Ayub, M.; Alsaedi, A. Mixed convective stagnation point flow of nanofluid with Darcy-Fochheimer relation and partial slip. *Results Phys.* **2018**, *9*, 771–778. [[CrossRef](#)]
9. Aghamajidi, M.; Yazdi, M.; Dinarvand, S.; Pop, I. Tiwari-Das nanofluid model for magnetohydrodynamics (MHD) natural-convective flow of a nanofluid adjacent to a spinning down-pointing vertical cone. *Propuls. Power Res.* **2018**, *7*, 78–90. [[CrossRef](#)]
10. Umavathi, J.C.; Hemavathi, K. Flow and heat transfer of composite porous medium saturated with nanofluid. *Propuls. Power Res.* **2019**, *8*, 173–181. [[CrossRef](#)]
11. Dero, S.; Rohni, A.M.; Saaban, A. The dual solutions and stability analysis of nanofluid flow using tiwari-das model over a permeable exponentially shrinking surface with partial slip conditions. *J. Eng. Appl. Sci.* **2019**, *14*, 4569–4582. [[CrossRef](#)]
12. Dogonchi, A.S.; Chamkha, A.J.; Hashemi-Tilehnoee, M.; Seyyedi, S.M.; Ganji, D.D. Effects of homogeneous-heterogeneous reactions and thermal radiation on magneto-hydrodynamic Cu-water nanofluid flow over an expanding flat plate with non-uniform heat source. *J. Cent. South Univ.* **2019**, *26*, 1161–1171. [[CrossRef](#)]
13. Benzema, M.; Benkahla, Y.K.; Labsi, N.; Ouyahia, S.-E.; El Ganaoui, M. Second law analysis of MHD mixed convection heat transfer in a vented irregular cavity filled with Ag-MgO/water hybrid nanofluid. *J. Therm. Anal. Calorim.* **2019**, *137*, 1113–1132. [[CrossRef](#)]
14. Sreedevi, P.; Reddy, P.S. Effect of magnetic field and thermal radiation on natural convection in a square cavity filled with TiO₂ nanoparticles using Tiwari-Das nanofluid model. *Alex. Eng. J.* **2021**, *61*, 1529–1541. [[CrossRef](#)]
15. Sreedevi, P.; Reddy, P.S.; Suryanarayana Rao, K.V. Effect of magnetic field and radiation on heat transfer analysis of nanofluid inside a square cavity filled with silver nanoparticles: Tiwari-Das model. *Waves Random Complex Media* **2021**, 1–19. [[CrossRef](#)]
16. Abel, M.S.; Tawade, J.V.; Shinde, J.N. The effects of MHD flow and heat transfer for the UCM fluid over a stretching surface in presence of thermal radiation. *Adv. Math. Phys.* **2012**, *2012*. [[CrossRef](#)]
17. Tian, X.-Y.; Li, B.-W.; Hu, Z.-M. Convective stagnation point flow of a MHD non-Newtonian nanofluid towards a stretching plate. *Int. J. Heat Mass Transf.* **2018**, *127*, 768–780. [[CrossRef](#)]
18. Rashid, I.; Sagheer, M.; Hussain, S. Entropy formation analysis of MHD boundary layer flow of nanofluid over a porous shrinking wall. *Phys. A Stat. Mech. Its Appl.* **2019**, *536*, 122608. [[CrossRef](#)]
19. Gopal, D.; Saleem, S.; Jagadha, S.; Ahmad, F.; Almatroud, A.O.; Kishan, N. Numerical analysis of higher order chemical reaction on electrically MHD nanofluid under influence of viscous dissipation. *Alex. Eng. J.* **2021**, *60*, 1861–1871. [[CrossRef](#)]
20. Othman, N.A.; Yacob, N.A.; Bachok, N.; Ishak, A.; Pop, I. Mixed convection boundary-layer stagnation point flow past a vertical stretching/shrinking surface in a nanofluid. *Appl. Therm. Eng.* **2017**, *115*, 1412–1417. [[CrossRef](#)]
21. Ziaei-Rad, M.; Kasaeipoor, A.; Mehdi Rashidi, M.; Lorenzini, G. A similarity solution for mixed-convection boundary layer nanofluid flow on an inclined permeable surface. *J. Therm. Sci. Eng. Appl.* **2017**, *9*. [[CrossRef](#)]
22. El-Shorbagy, M.A.; Eslami, F.; Ibrahim, M.; Barnoon, P.; Xia, W.-F.; Toghraie, D. Numerical investigation of mixed convection of nanofluid flow in a trapezoidal channel with different aspect ratios in the presence of porous medium. *Case Stud. Therm. Eng.* **2021**, *25*, 100977. [[CrossRef](#)]
23. Chamkha, A.J.; Aly, A.M.; Al-Mudhaf, H.F. Laminar MHD mixed convection flow of a nanofluid along a stretching permeable surface in the presence of heat generation or absorption effects. *Int. J. Microscale Nanoscale Therm. Fluid Transp. Phenom.* **2011**, *2*, 51.
24. Matin, M.H.; Nobari, M.R.H.; Jahangiri, P. Entropy analysis in mixed convection MHD flow of nanofluid over a non-linear stretching sheet. *J. Therm. Sci. Technol.* **2012**, *7*, 104–119. [[CrossRef](#)]
25. Ibrahim, S.M.; Lorenzini, G.; Kumar, P.V.; Raju, C.S.K. Influence of chemical reaction and heat source on dissipative MHD mixed convection flow of a Casson nanofluid over a nonlinear permeable stretching sheet. *Int. J. Heat Mass Transf.* **2017**, *111*, 346–355. [[CrossRef](#)]
26. Vasanthakumari, R.; Pondy, P. Mixed convection of silver and titanium dioxide nanofluids along inclined stretching sheet in presence of MHD with heat generation and suction effect. *Math. Model. Eng. Probl.* **2018**, *5*, 123–129. [[CrossRef](#)]
27. Gupta, S.; Kumar, D.; Singh, J. MHD mixed convective stagnation point flow and heat transfer of an incompressible nanofluid over an inclined stretching sheet with chemical reaction and radiation. *Int. J. Heat Mass Transf.* **2018**, *118*, 378–387. [[CrossRef](#)]
28. Devi, S.S.U.; Devi, S.P.A. Numerical investigation of three-dimensional hybrid Cu-Al₂O₃/water nanofluid flow over a stretching sheet with effecting Lorentz force subject to Newtonian heating. *Can. J. Phys.* **2016**, *94*, 490–496. [[CrossRef](#)]
29. Waini, I.; Ishak, A.; Pop, I. Flow and heat transfer of a hybrid nanofluid past a permeable moving surface. *Chin. J. Phys.* **2020**, *66*, 606–619. [[CrossRef](#)]
30. Zainal, N.A.; Nazar, R.; Naganthran, K.; Pop, I. MHD mixed convection stagnation point flow of a hybrid nanofluid past a vertical flat plate with convective boundary condition. *Chin. J. Phys.* **2020**, *66*, 630–644. [[CrossRef](#)]
31. Waini, I.; Ishak, A.; Groşan, T.; Pop, I. Mixed convection of a hybrid nanofluid flow along a vertical surface embedded in a porous medium. *Int. Commun. Heat Mass Transf.* **2020**, *114*, 104565. [[CrossRef](#)]
32. Rostami, M.N.; Dinarvand, S.; Pop, I. Dual solutions for mixed convective stagnation-point flow of an aqueous silica-alumina hybrid nanofluid. *Chin. J. Phys.* **2018**, *56*, 2465–2478. [[CrossRef](#)]

33. Jamaludin, A.; Naganthran, K.; Nazar, R.; Pop, I. MHD mixed convection stagnation-point flow of Cu-Al₂O₃/water hybrid nanofluid over a permeable stretching/shrinking surface with heat source/sink. *Eur. J. Mech.* **2020**, *84*, 71–80. [[CrossRef](#)]
34. Khashi'ie, N.S.; Arifin, N.M.; Pop, I. Non-Darcy mixed convection of hybrid nanofluid with thermal dispersion along a vertical plate embedded in a porous medium. *Int. Commun. Heat Mass Transf.* **2020**, *118*, 104866. [[CrossRef](#)]
35. Waini, I.; Ishak, A.; Pop, I. Unsteady flow and heat transfer past a stretching/shrinking sheet in a hybrid nanofluid. *Int. J. Heat Mass Transf.* **2019**, *136*, 288–297. [[CrossRef](#)]
36. Khashi'ie, N.S.; Arifin, N.M.; Pop, I.; Nazar, R.; Hafidzuddin, E.H.; Wahi, N. Three-dimensional hybrid nanofluid flow and heat transfer past a permeable stretching/shrinking sheet with velocity slip and convective condition. *Chin. J. Phys.* **2020**, *66*, 157–171. [[CrossRef](#)]
37. Anuar, N.S.; Bachok, N.; Pop, I. Influence of buoyancy force on Ag-MgO/water hybrid nanofluid flow in an inclined permeable stretching/shrinking sheet. *Int. Commun. Heat Mass Transf.* **2021**, *123*, 105236. [[CrossRef](#)]
38. Roşca, N.C.; Pop, I. Hybrid nanofluids flows determined by a permeable power-Law stretching/shrinking sheet modulated by orthogonal surface shear. *Entropy* **2021**, *23*, 813. [[CrossRef](#)] [[PubMed](#)]
39. Anuar, N.S.; Bachok, N.; Pop, I. Cu-Al₂O₃/water hybrid nanofluid stagnation point flow past MHD stretching/shrinking sheet in presence of homogeneous-heterogeneous and convective boundary conditions. *Mathematics* **2020**, *8*, 1237. [[CrossRef](#)]
40. Wahid, N.S.; Arifin, N.M.; Khashi'ie, N.S.; Pop, I. Hybrid nanofluid slip flow over an exponentially stretching/shrinking permeable sheet with heat generation. *Mathematics* **2021**, *9*, 30. [[CrossRef](#)]
41. Waini, I.; Ishak, A.; Pop, I. Transpiration effects on hybrid nanofluid flow and heat transfer over a stretching/shrinking sheet with uniform shear flow. *Alexandria Eng. J.* **2020**, *59*, 91–99. [[CrossRef](#)]
42. Afridi, M.I.; Qasim, M.; Khan, I.; Shafie, S.; Alshomrani, A.S. Entropy generation in magnetohydrodynamic mixed convection flow over an inclined stretching sheet. *Entropy* **2017**, *19*, 10. [[CrossRef](#)]
43. Abu-Libdeh, N.; Redouane, F.; Aissa, A.; Mebarek-Oudina, F.; Almuhtady, A.; Jamshed, W.; Al-Kouz, W. Hydrothermal and entropy investigation of Ag/MgO/H₂O hybrid nanofluid natural convection in a novel shape of porous cavity. *Appl. Sci.* **2021**, *11*, 1722. [[CrossRef](#)]
44. Khan, U.; Zaib, A.; Abu Bakar, S.; Ishak, I. Stagnation-point flow of a hybrid nanofluid over a non-isothermal stretching/shrinking sheet with characteristics of inertial and microstructure. *Case Stud. Therm. Eng.* **2021**, *26*, 101150. [[CrossRef](#)]
45. Ghalambaz, M.; Doostani, A.; Izadpanahi, E.; Chamkha, A.J. Conjugate natural convection flow of Ag-MgO/water hybrid nanofluid in a square cavity. *J. Therm. Anal. Calorim.* **2020**, *139*, 2321–2336. [[CrossRef](#)]
46. Esfe, M.H.; Arani, A.A.A.; Rezaie, M.; Yan, W.-M.; Karimipour, A. Experimental determination of thermal conductivity and dynamic viscosity of Ag-MgO/water hybrid nanofluid. *Int. Commun. Heat Mass Transf.* **2015**, *66*, 189–195. [[CrossRef](#)]
47. Merkin, J.H. On dual solutions occurring in mixed convection in a porous medium. *J. Eng. Math.* **1986**, *20*, 171–179. [[CrossRef](#)]
48. Weidman, P.D.; Kubitschek, D.G.; Davis, A.M.J. The effect of transpiration on self-similar boundary layer flow over moving surfaces. *Int. J. Eng. Sci.* **2006**, *44*, 730–737. [[CrossRef](#)]
49. Harris, S.D.; Ingham, D.B.; Pop, I. Mixed convection boundary-layer flow near the stagnation point on a vertical surface in a porous medium: Brinkman model with slip. *Transp. Porous Media* **2009**, *77*, 267–285. [[CrossRef](#)]
50. Shampine, L.F.; Gladwell, I.; Shampine, L.; Thompson, S. *Solving ODEs with Matlab*; Cambridge University Press: Cambridge, UK, 2003; ISBN 0521530946.
51. Roşca, A.V.; Pop, I. Flow and heat transfer over a vertical permeable stretching/shrinking sheet with a second order slip. *Int. J. Heat Mass Transf.* **2013**, *60*, 355–364. [[CrossRef](#)]
52. Spangenberg, W.G.; Rowland, W.R.; Mease, N.E. *Fluid Mechanics of Internal Flows*; Elsevier: Amsterdam, The Netherlands, 1967.
53. Aidun, C.K.; Triantafillopoulos, N.G.; Benson, J.D. Global stability of a lid-driven cavity with throughflow. *Phys. Fluids* **1991**, *A3*, 2081–2091. [[CrossRef](#)]
54. Ishak, A.; Merkin, J.H.; Nazar, R.; Pop, I. Mixed convection boundary layer flow over a permeable vertical surface with prescribed wall heat flux. *Z. Angew. Math. Phys.* **2008**, *59*, 100–123. [[CrossRef](#)]